Journal of Inorganic and General Chemistry
ZAAC
Zeitschrift für anorganische und allgemeine Chemie
DOI: 10.1002/zaac.201900269
ARTICLE

Investigations on Tetragonally Distorted Sodium Thallide NaTl-*tI*8

Susanne M. Tiefenthaler,[a] Marc Schlosser,[a] Florian Pielnhofer,[a] Ilya G. Shenderovich,[b] Arno Pfitzner,[a] and Stefanie Gärtner*[a,b]

Dedicated to Prof. Dr. H. J. Deiseroth on the Occasion of his 75th Birthday

Abstract. In-depth investigations of the long-time known Zintl phase NaTl revealed a phase transition of tetragonal NaTl-*tI*8 [$I4_1/amd$; a = 5.2268(9) Å, c = 7.539(1) Å, V = 205.97(9) Å^3] to Zintl's cubic NaTl-*cF*16 [$Fd\bar{3}m$; a = 7.4697(6) Å, V = 416.79(5) Å^3] between 351 and 355 K. This phase transformation was observed for NaTl prepared by two different synthetic routes including Zintl's original procedure. An excess of sodium applied during the synthesis in liquid ammonia also resulted in the formation of NaTl-*tI*8. DSC measurements suggest a first order phase transition. In addition to in-situ temperature dependent powder X-ray diffraction experiments, DSC measurements and solid-state NMR investigations, we also performed theoretical DOS and band structure calculations for the cubic and tetragonal phase, respectively. The results suggest Na-Tl interactions in the second coordination sphere being responsible for the observed tetragonal distortion of Zintl's cubic NaTl.

Introduction

The direct reduction of the late main group elements, respectively their halides, in liquid ammonia by alkali metal represents an elegant way to obtain polar intermetallics of these elements at low temperature.[1] In 1932, *E. Zintl* reported on the crystal structure of NaTl, which he determined from powder diffraction data.[2] From his data, he rightly concluded a cubic compound crystallizing in the cubic space group $Fd\bar{3}m$, where the sodium as well as the thallium substructure form a diamond-like tetrahedral network. This result nicely supported the pseudo atom rationalization introduced by *Klemm* in 1944.[3] A closer look at the alkali metal – thallium system shows that the NaTl structure, which one would unsophisticatedly expect to be the same for any 1 : 1 alkali metal thallide, is rather an exception than a common structural motif for this class of compounds at ambient conditions.

In greater detail, LiTl can be regarded as an ionic compound crystallizing in the CsCl-structure type,[4] whereas in KTl and CsTl octahedrally shaped Tl_6^{6-} anions are present.[5] *Miller* et al. could show that the pseudoatom rationalization is not appropriate to describe the structure formation according to the 8–N rule in alkali metal thallides, as NaTl is the only representative where this concept works.[6] LiTl may be regarded as a classical ionic compound, whereas KTl and CsTl form structures lower in symmetry at ambient conditions including octahedrally shaped Tl_6^{6-} anions where the octet rule formally remains valid. In general, the nature of A(I)B(III) phases (A = alkali metal, B = group 13 element) is reported to be dependent on the pressure applied during synthesis.[7] The NaTl-*cF*16 type structures of the heavier alkali metals (K-Cs) only are stable at high pressures.[7,8] In the alkali metal - trielide system, temperature dependent phase transitions have been reported for LiIn and LiAl, which both crystallize in the NaTl-type structure (cubic, $Fd\bar{3}m$) at room temperature.[9] At lower temperatures (93 K for LiAl, and 170 K for LiIn), a reversible phase transition into the body centered tetragonal space group ($I4_1/amd$) occurs. The phase transition between the structures crystallizing in the translationengleiche space groups is reported only for lithium deficient LiAl and LiIn.[10]

Recently, we reported on NaTl crystallizing in a tetragonal crystal structure stable at room temperature, by using different synthetic routes (via reducing Tl^I salts by sodium in liquid ammonia as well as classical solid state techniques from the elements). Powder diffraction patterns of samples revealed the same characteristic splitting of reflections due to tetragonal symmetry.[11] Previously, this tetragonal distortion was correlated to sodium vacancies in NaTl by synchrotron powder diffraction studies[12] and alternatively a cation short-range order of non-stoichiometric NaTl was suggested.[13]

In the crystal structure of tetragonally distorted NaTl, the longer crystallographically independent Na-Tl distance in Zintl's cubic description (3.731 Å) splits into two slightly different distances (3.701 Å and 3.764 Å). The Na–Na distances as well as the Tl–Tl distances are not significantly affected. For the tetrahedral environment of thallium and sodium,

* Dr. S. Gärtner
E-Mail: Stefanie.Gaertner@ur.de
* Institute of Inorganic Chemistry
University of Regensburg
93040 Regensburg, Germany
* Central Analytics
Faculty of Chemistry and Pharmacy
University of Regensburg
93040 Regensburg, Germany
Supporting information for this article is available on the WWW under **http://dx.doi.org/10.1002/zaac.201900269** or from the author.

respectively, only a slight distortion from the ideal tetrahedral angle is observed.

Herein, we present more detailed investigations on tetragonally distorted NaTl-*tI*8 derived by two synthetic methods, firstly high temperature solid state reaction and secondly Zintl's procedure at low temperature in liquid ammonia. Hereby, temperature-dependent powder X-ray diffraction methods, DSC measurements and ^{23}Na solid state NMR spectroscopy have been applied.In order to gain deeper insights into the reasons for the stability of the tetragonal phase, we additionally performed theoretical band structure calculations.

Results and Discussion

Heating of a sample of tetragonal NaTl-*tI*8[11] revealed a change in the diffraction pattern, as the split lines fall together and fit the cubic cell of Zintl's NaTl-*cF*16 (Figure 1, for indexed lines please see Supporting Information).

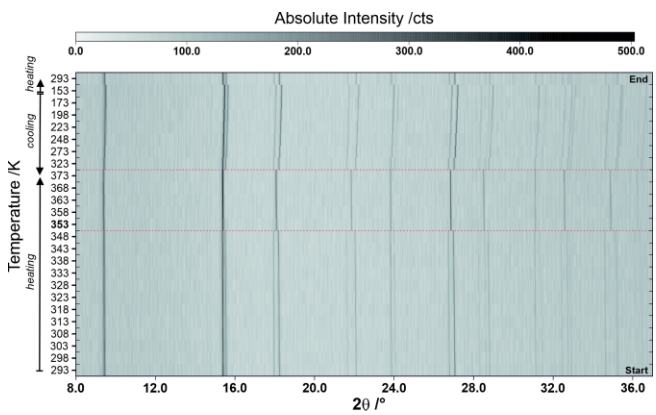

Figure 1. Compilation of temperature-dependent top view PXRD patterns (λ = 0.70926 Å, Mo-$K_{\alpha1}$) of NaTl: heating from room temperature to 373 K, then cooling down to 153 K and finally reheating to room temperature. The reversible phase transition from tetragonal NaTl-*tI*8 to cubic NaTl-*cF*16 and vice versa at approx. 353 K is marked with dotted lines (red).

Smaller heating steps between 351 and 355 K reveal a phase transition from tetragonal $I4_1/amd$ NaTl-*tI*8 to cubic $Fd\bar{3}m$ NaTl-*cF*16 (Figure 2). Due to the coexistence of both phases at 353 K, we presumed a first order phase transition, which was confirmed by associated heat anomalies during heating and cooling steps in DSC measurements (Figure 3). The endothermic peak upon heating occurs at 355 K, whereas cooling of the sample gives a temperature of 351 K for the beginning of the phase transformation [onset: 358 K (heating), 350 K (cooling)]. The integrated regions suggest a small transition entropy in the magnitude of 1 J·mol^{-1}·K^{-1} per formula unit NaTl. The nature of the phase transition belonging to the first order type is also supported by the discontinuity in the temperature dependent lattice parameters at the transition temperature (see SI-Figure 2, Supporting Information).

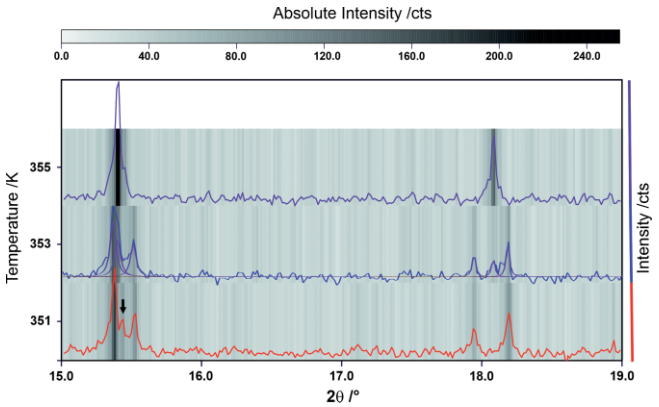

Figure 2. Compilation of temperature-dependent PXRD patterns, superimposed with top view patterns (λ = 0.70926 Å, Mo-$K_{\alpha1}$) of NaTl in a narrow temperature range around the phase change temperature showing the tetragonal NaTl-*tI*8 phase at 351 K and the cubic NaTl-*cF*16 phase at 355 K. At 353 K Bragg reflections of both phases are visible in the powder pattern, highlighted by a suitable profile function (violet). The additional reflection at 2θ = 15.5° (arrow) is due to impurities derived by the previously prepared NMR sample, where the same material was used.

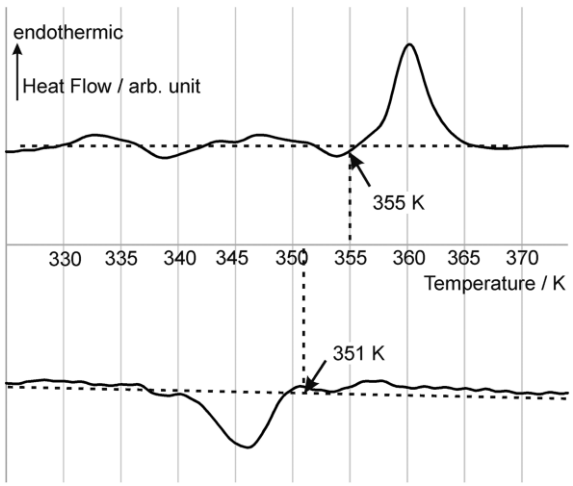

Figure 3. DSC results upon heating and cooling of NaTl (10 K·min^{-1}).

The phase transition also occurs in multiple samples of sodium thallide, produced by the low temperature route of dissolving sodium in liquid ammonia in the presence of thallium(I) salts. The temperature dependence of the product obtained by the reaction of thallium(I)-bromide and sodium is shown in Figure 4. The splitting of reflections due to the presence of NaTl-*tI*8 is evident. The additional reflections compared to the sample prepared by the high temperature route are due to elemental thallium, which is formed during the washing out progress for removing NaBr.

We also prepared a sample with a large excess of sodium during the direct reduction experiments in liquid ammonia (for details please the see experimental section), which also resulted in the formation of NaTl-*tI*8 (for PXRD pattern see SI-Figure 3, Supporting Information). Here, Tl is also present due to the washing out progres for removing NaBr. Besides Tl

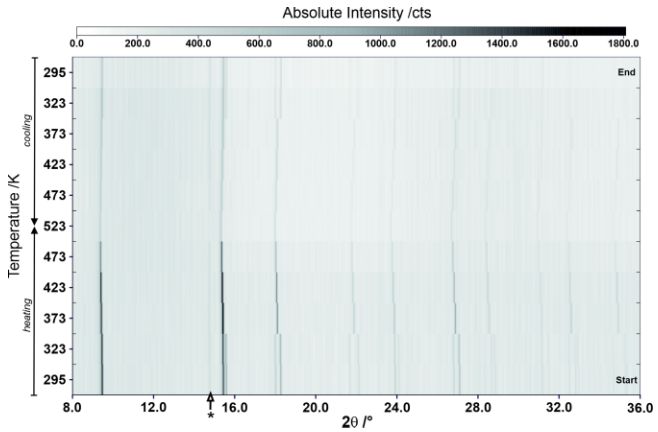

Figure 4. Compilation of temperature-dependent top view PXRD patterns (λ = 0.70926 Å, Mo-$K_{\alpha 1}$) of NaTl prepared by Zintl's route. The additional reflection at 14.8 2Θ (arrow) is due to elemental thallium.

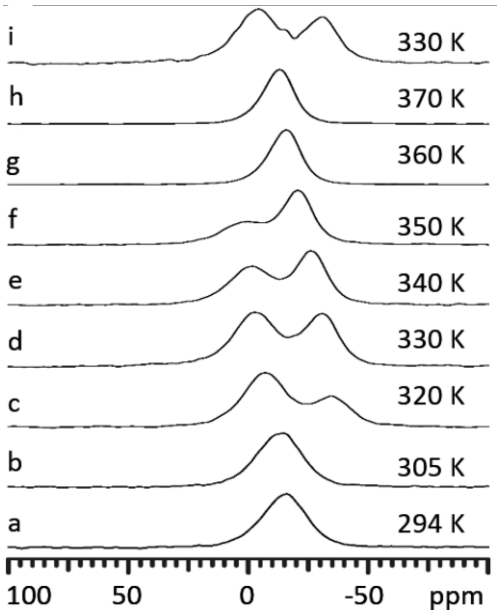

Figure 5. Temperature dependent ^{23}Na solid-state MAS NMR spectra of NaTl.

small amounts of NaBr are present, and additionally new reflections occur, which we attribute to the presence of a not yet further characterized product. In literature, a reactivity for the lighter homologue indium is reported, where InI_3 and KNH_2 form $In(NH_2)_3$ in liquid ammonia. If LiI is additionally present, $Li_3In(NH_2)_6$ is formed.[14] The formation of $NaNH_2$ in our experimental setup is obvious; therefore, we presume an amido thallium species being responsible for the observed additional reflections. In principle, our result demonstrates that the formation of tetragonally distorted NaTl-*tI*8 in liquid ammonia solutions is independent from the sodium concentration. The exact chemical composition of our compounds cannot be determined by the methods applied, therefore sodium deficiency is also conceivable.[10,12]

Since X-ray diffraction methods only work on crystalline materials, ^{23}Na solid state NMR was employed as an additional method for investigating the structure of NaTl during the phase transition. ^{23}Na NMR spectra of NaTl were measured in the temperature range from 294 K to 370 K (the results of the deconvolution of these spectra are summarized in SI-Table 2, Supporting Information). The characteristic spectral changes are shown in Figure 5. While at 294 K the ^{23}Na NMR spectrum shows only one peak at –14.7 ppm, at 315 K a second peak appears at a higher field. With rising temperatures, the relative intensities of the peaks vary and as a result, only the second peak remains detectable at –15.2 ppm (360 K and above).

Taking into account the evidence of the reversible phase transition demonstrated by the powder diffraction experiments mentioned above, we attribute the first peak to the tetragonal phase while ascribing the second one to the cubic phase. The similarity in the chemical shifts (–14.7 and –15.2 ppm) when one phase is exclusively present, is supported by the very similar crystal structures of both tetragonal and cubic phase. The variations of the molar fractions of the peak we associate with the tetragonal, respectively cubic phase with temperature are shown in Figure 6, which also reflects the coexistence of both phases between 320 K and 360 K. The temperature range when both phases coexist is larger than the small phase transition temperature range in the crystalline part during powder XRD experiments (351–355 K). One possible explanation would be the involvement of an amorphous part of NaTl without any long-range order.

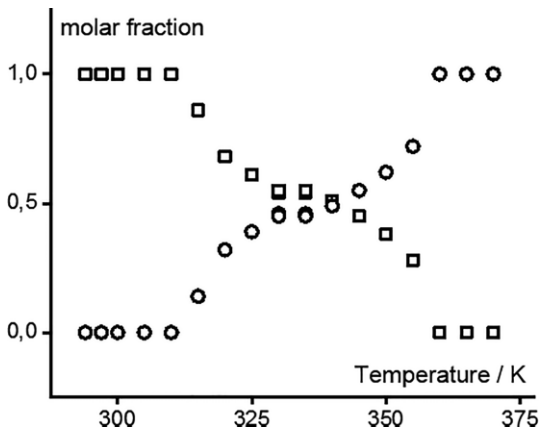

Figure 6. The temperature dependence of the molar fractions of the tetragonal (□) and cubic (○) phases of NaTl as obtained from the NMR spectroscopic data.

The chemical shifts of both peaks increase slightly upon heating (Figure 7), however the dependence of the chemical shift on temperature cannot always be associated with a phase transition.[15] Nevertheless, the shape of the observed dependence suggests the presence of a direct effect of the two phases on the structure of each other, of course the presence of quadrupolar effects of ^{23}Na must also be taken into account. Further investigations involving ^{23}Na and ^{205}Tl MAS NMR are planned to elucidate ongoing processes in NaTl.

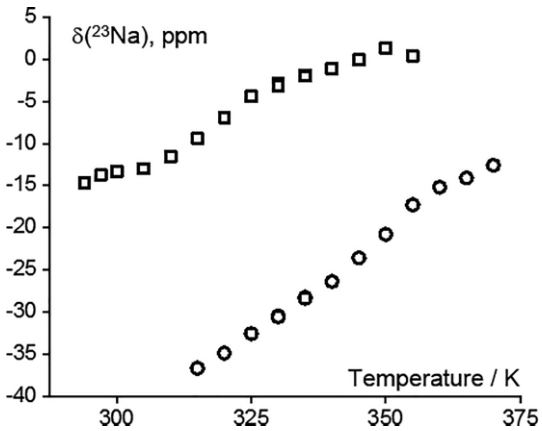

Figure 7. The temperature dependence of the first (□) and the second (○) peaks of the ^{23}Na solid-state MAS NMR spectra of NaTl.

Since the experiments give insight into the structural changes of NaTl during the phase transition, but do not explain the observed temperature dependent change in the crystal structure of the latter, we additionally performed theoretical band structure calculations on the stoichiometric NaTl phase. Miller et al. have shown that the ionic picture for NaTl is not precise due to significant Na contributions below E_F in the density of states.[6] In addition, they demonstrated that the covalent Tl-Tl interaction is optimized because the Fermi level is positioned at the bonding-antibonding crossover of the Crystal Orbital Hamilton Population (COHP) curve. One sodium–thallium distance would be expected by applying the classical Zintl Klemm concept of a covalently bound sublattice interacting with sodium cations "innocently", in terms of exclusively electrostatic interaction, resulting in the highest possible cubic symmetry. The reduction in symmetry in the tetragonal phase is predominantly caused by Na–Tl interactions in the second coordination sphere. However, *Miller* et al. have considered only the nearest neighbour (nn) interactions in the COHP curves. As mentioned above, the tetragonal distortion of the NaTl structure results in a splitting of the next nearest neighbour (nnn) Na–Tl distances, while there is no change for *d*(Tl–Tl) and *d*(Na–Na). When these nnn interactions are taken into account, the COHP curves have to be extended (see Figure 8). The splitting of the nnn Na–Tl distances as obtained by DFT (3.681 Å and 3.810 Å) is slightly larger than the experimental values. The non-split nnn distances in the cubic form (3.723 Å) are in good agreement with the experimental value. Almost no differences are observed when comparing the nn Na–Tl interactions in the COHP curves for both cubic and tetragonal structures. A different situation is obtained for the second coordination sphere: The integrated COHP (ICOHP) value of 5.7 kJ·mol^{-1} for the tetragonal structure (3.681 Å and 3.810 Å) is slightly larger than 2.7 kJ·mol^{-1} for the cubic structure (3.723 Å). This indicates that the splitting of the nnn Na–Tl distances is optimized in the tetragonal structure due to stronger Na–Tl bonding interactions. Note that a more positive value means a stronger bonding in this context. The very small, but still observed total energy difference of 0.14 kJ·mol^{-1} between tetragonal and cubic NaTl also supports the stability of the tetragonally distorted phase of NaTl.

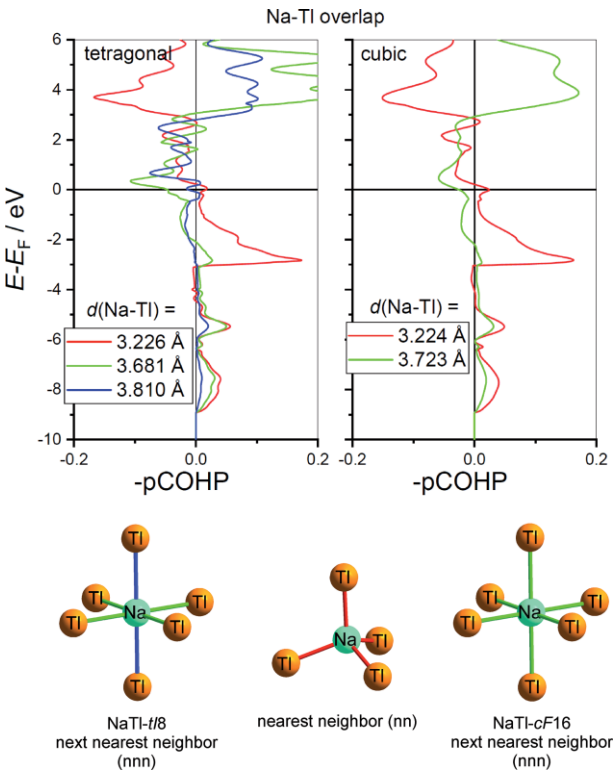

Figure 8. COHP curves of the nn and nnn Na–Tl interactions in the cubic and tetragonal structure of NaTl.

Conclusions

We prepared a tetragonal phase of NaTl by two synthetic methods, a high temperature solid state reaction as well as a low temperature solution route in liquid ammonia. A stoichiometric approach as well as an excess of sodium during the low temperature preparation did not result in Zintl's cubic compound. The tetragonal phase NaTl-*tI*8 ($I4_1/amd$) transforms into Zintl's cubic NaTl-*cF*8 ($Fd\bar{3}m$) structure via a reversible first order transformation between the translationengleiche space groups (351–355 K). In addition to temperature-dependent powder X-ray diffraction analyses, solid-state ^{23}Na NMR spectra of the sample prepared at high temperature were recorded, which also confirmed the reversible transformation. DSC measurements proved the presence of a first order phase transition, which is supported by the observation of the coexistence of both phases at 353 K. Theoretical calculations helped to find a reason for the phase transition. The splitting of the nnn distances results in an optimization of the Na–Tl bonding interactions and stabilizes the tetragonal structure even for stoichiometric 1:1 NaTl. The observation of NaTl-*tI*8 during the employment of excess sodium during direct reduction experiments emphasizes the favoured formation of the latter in liquid ammonia compared to cubic NaTl-*cF*16.

Experimental Section

For preparation details of NaTl, please see reference [12].

Sodium thallide was prepared via direct reduction in accordance with Zintl's reports. For the amounts used for the stoichiometric reactions, please see reference [11].

For the direct reduction of TlBr with an excess of sodium, TlBr (70 mg, 0.246 mmol) and sodium (16.9 mg, 0.739 mmol) were placed in a heated Schlenk tube. Subsequent condensation of dried ammonia onto the reactants led to a blue solution. After ten months storage at 233 K, the solution had turned colorless. The ammonia was evaporated and the black and white residue dried under vacuum and stored in an argon filled glovebox.

In order to obtain information on the phase transition via DCS, in a glovebox, 19.6 mg of NaTl were filled into an aluminum crucible, which was subsequently clamped shut. The sample was heated in a continuous nitrogen flow, from 298 K to 393 K and cooled back down to 298 K with a heating and cooling rate of 10 $K \cdot min^{-1}$. All measurements were performed on a METTLER TOLEDO DSC (METTLER TOLEDO, Gießen, Germany) with a DSC30 measuring cell, with the software METTLER TOLEDO STAR^e 5.1 used for evaluation purposes.

For analysis via X-ray powder diffraction, glass capillaries with a diameter of 0.3 mm were filled with the finely ground reaction product and sealed by melting. All powder data were recorded on a STADI P diffractometer (STOE & Cie GmbH, Darmstadt, Germany), with the software WinXPOW (STOE & Cie GmbH, Darmstadt, Germany) used for visualization and indexation purposes.[16] Temperature dependent measurement was performed using a Cryostream 700 (Oxford Cryosystems, Oxford, UK).

The solid-state ^{23}Na NMR measurements were performed on an Infinity$_{plus}$ spectrometer system (Agilent) operated at 7 T, equipped with a variable–temperature Chemagnetics–Varian 6 mm pencil cross polarization magic angle spinning (CPMAS) probe. The spectra were recorded using magic angle spinning (MAS) rates of about 6 kHz, a 90° pulse of 4.0 µs, and the relaxation delay of 1 s. The spectra were indirectly referenced to NaCl (1 M in H_2O). At each temperature point, the sample was thermostatted for 10 min before the measurement. The numerical NMR parameters were extracted from the experimentally obtained spectra using the WSolids1 program package.[17]

DFT Calculations: Quantum chemical calculations were performed in the framework of density functional theory (DFT) using a linear combination of Gaussian-type functions (LCGTF) Scheme as implemented in CRYSTAL17.[18] Full structural optimizations were carried out with the Vosko-Wilk-Nusair (VWN) parametrization of the local density approximation LDA.[19] The convergence criterion considering the energy was set to 1×10^{-10} a.u. with a k-mesh sampling of $12 \times 12 \times 12$. The basis sets for Na and Tl were taken from [20]

Supporting Information (see footnote on the first page of this article): More details for the temperature dependent powder diffraction experiments, a powder pattern of the product obtained by Zintl′s route, and the temperature dependent evolution of chemical shifts in the NMR spectra.

Acknowledgements

S.T. and S.G. thank *Prof. N. Korber* for providing materials and lab equipment as wells as for valuable discussions. F.P. thanks *Prof. Bettina Lotsch*, *Dr. Ulrich Wedig* and the Computer Service group from the Max-Planck-Institute for Solid State Research (Stuttgart, Germany) for access to CRYSTAL17 and computational facilities. The authors thank *Ulrike Schießl* for DSC measurements.

Keywords: Sodium thallide; Zintl phases; Phase transitions; ^{23}Na solid state MAS NMR; Band structure

References

[1] E. Zintl, A. Harder, *Z. Phys. Chem. Abt. A* **1931**, 47–91; E. Zintl, J. Goubeau, W. Dullenkopf, *Z. Phys. Chem.* **1931**, *154*, 1–46; E. Zintl, H. Kaiser, *Z. Anorg. Allg. Chem.* **1933**, *211*, 113–131; S. Gaertner, N. Korber, in *Zintl Ions Principles and Recent Developments, Vol. 140* (Ed.: T. F. Faessler), Springer-Verlag, Berlin Heidelberg, Germany, **2011**, pp. 25–56; S. Gaertner, N. Korber, in *Comprehensive Inorganic Chemistry II* (second edition) (Eds.: J. Reedijk, K. Poeppelmeier), Elsevier, Amsterdam, **2013**, pp. 251–267; S. M. Kauzlarich, *Chemistry, Structure and Bonding of Zintl Phases and Ions*, VCH Publishers, Inc., New York, Weinheim, Cambridge, **1996**.
[2] E. Zintl, W. Dullenkopf, *Z. Phys. Chem. B* **1932**, *16*, 195–205; E. Zintl, A. Harder, S. Neumayr, *Z. Phys. Chem. A* **1931**, *154*, 92–96.
[3] R. Nesper, *Z. Anorg. Allg. Chem.* **2014**, *640*, 2639–2648.
[4] W. Baden, P. C. Schmidt, A. Weiss, *Phys. State Sol. A* **1979**, *51*, 183–190.
[5] Z. C. Dong, J. D. Corbett, *J. Am. Chem. Soc.* **1993**, *115*, 11299–11303; Z. C. Dong, J. D. Corbett, *Inorg. Chem.* **1996**, *35*, 2301–2306.
[6] G. J. Miller, M. W. Schmidt, F. Wang, T. You, in *Zintl Phases – Principles and Recent Developments*, vol. 139 (Ed.: T. F. Faessler), Springer-Verlag, Berlin Heidelberg, **2011**, pp. 1–56.
[7] J. Evers, in *Zintl Phases – Principes and Recent Developments*, vol. 139 (Ed.: T. F. Faessler), Springer-Verlag, Berlin Heidelberg, **2011**, pp. 57–96.
[8] J. Evers, G. Oehlinger, *Inorg. Chem.* **2000**, *39*, 628–629.
[9] H. Ehrenberg, H. Pauly, T. Hansen, J. C. Jaud, H. Fuess, *J. Solid State Chem.* **2002**, *167*, 1–6; H. Ehrenberg, H. Pauly, M. Knapp, J. Grobner, D. Mirkovic, *J. Solid State Chem.* **2004**, *177*, 227–230.
[10] E. Vollmar, H. Ehrenberg, M. Knapp, C. Baehtz, H. Pauly, *HASYLAB Ann. Rep.* **2004**, 551–552.
[11] S. Tiefenthaler, N. Korber, S. Gaertner, *Materials* **2019**, *12*, 1356–1366.
[12] E. Vollmar, H. Ehrenberg, C. Baehtz, M. Knapp, H. Pauly, *HASYLAB Ann. Rep.* **2005**, 533–534.
[13] J. Schneider, *Mater. Sci. Forum* **1988**, *27/28*, 63–68.
[14] A. P. Purdy, *Inorg. Chem.* **1994**, *33*, 282–286.
[15] B. C. K. Ip, I. G. Shenderovich, P. M. Tolstoy, J. Frydel, G. S. Denisov, G. Buntkowsky, H. Limbach, *J. Phys. Chem. A* **2012**, *116*, 11370–11387; E. Y. Tupikina, M. Bodensteiner, P. M. Tolystoy, G. S. Denisov, I. G. Shenderovich, *J. Phys. Chem. C* **2018**, *122*, 1711–1720.
[16] STOE, in *STOE WinXPOW, Vol. 3.0.2.1*, STOE & Cie 2000 Darmstadt, Darmstadt, Germany, **2011**, p. Powder Diffraction Software.
[17] K. Eichele, WSolids ver.1.20.20., Universität Tübingen, Germany **2013**.
[18] R. Dovesi, A. Erba, R. Orlando, C. M. Zicovich-Wilson, B. Civalleri, L. Maschio, M. Rérat, S. Casassa, J. Baima, S. Salustro, B. Kirtman, *Wiley Interdiscip. Rev. Comput. Mol. Sci.* **2018**, *8*, e1360; R. Dovesi, V. R. Saunders, C. Roetti, R. Orlando, C. M. Zicovich-Wilson, F. Pascale, B. Civalleri, K. Doll, N. M. Harrison, I. J. Bush, P. D′Arco, M. Llunell, M. Causà, Y. Noël, L.

Maschio, A. Erba, M. Rerat, S. Casassa, University of Torino, Torino, **2017**.
[19] S. H. Vosko, L. Wilk, M. Nusair, *Can. J. Phys.* **1980**, *58*, 1200–1211.
[20] G. Sophia, P. Baranek, C. Sarrazin, M. Rerat, R. Dovesi, *Phase Trans.* **2013,** *81*, 1069; F. Bachhuber, I. Anusca, J. Rothballer, F. Pielnhofer, P. Peter, R. Weihrich, *Solid State Sci.* **2011**, *13*, 337–343.

Received: October 30, 2019
Published Online: January 15, 2020

